Model-Based Nonlinear Control of a Class of Musculoskeletal Systems

Model-Based Nonlinear Control of a Class of Musculoskeletal Systems

Raphael Stolpe, Yannick Morel

Abstract— **The presented work addresses the motion control problem for a class of musculoskeletal systems, composed of the combination of a rigid multibody system (i.e. the *skeletal* part) subjected to efforts produced by a set of muscle-tendon complexes. A control law, prescribing the rate of change of muscle fiber activation, is proposed and shown to guarantee exponential convergence of skeletal joint angles to user-defined desired trajectories. Results of numerical simulations, for a simple two degree of freedom skeletal system actuated by five muscle-tendon complexes, illustrate efficacy of the approach.**

I. Introduction

The nervous system has evolved to become, among other qualities, a distinctly capable controller of movements ([1, 2]). This functional ability of the neural circuitry responsible to support motion control tasks, combined with the mechanical properties of muscle-tendon complexes it is acting upon, has afforded humans a degree of robustness and compliance in their movements that is essential to supporting compliant mechanical interactions with their surroundings, qualities that have largely eluded actuated artificial agents. Emulating such qualities on robotic systems would prove of benefit to numerous applications. However, our knowledge of the manner in which the nervous system solves control problems remains limited, for instance as pertains to how the multitude of brain regions involved in motor control functionally interact ([3]). The development of motion control technology addressing the same types of control problems can prove helpful in advancing this knowledge. Consideration of such control algorithms, and more specifically of the closed-loop dynamical properties obtained when they are applied to the corresponding physical systems (or models thereof), can be exploited to constrain computational neural models descriptive of sensorimotor loops. This notion of dynamical functional constraining constitutes a natural extension of the well-established concept of physical grounding, or embodiment (see the discussion in [4-7]). A particularly promising approach in this perspective would be to construct and subsequently study such a motion controller *in vivo*.

Recent advances in neurotechnology have allowed to investigate the restoration of voluntary movement in humans with spinal cord injury ([8, 9]). The method utilizes Epidural Electrical Stimulation (EES) to stimulate motor neuron pools with spatiotemporal patterns ([8-10]). Specifically, a closed-loop controller is constructed from previously recorded ElectroMyoGraphic (EMG) activity. Emulating the activity corresponding to a foot trajectory, and applying it through EES ([8, 9, 11-13]), one is able to elicit a voluntary sequence of actions supporting a walking pattern. The control framework applied in [8] and [9] however remains largely naive to the neuromuscular dynamics supporting actuation of human legs. In effect, it essentially amounts to the replaying of prerecorded input trajectories, modulated in real-time to pursue effectiveness. While this approach has shown outstanding results, improvements to the control design could be expected to result in greater quality of achieved movements.

Simple, relevant approaches include Proportional Integral Derivative (PID) control ([14, 15]). However, muscle-tendon dynamics are characterized by a strongly nonlinear behavior ([16-18]), limiting the expected effectiveness of linear control techniques. Neural control approaches have been successfully applied to address the control of neuromusculoskeletal systems. In [19], for instance, the authors propose the use of a neural network to control the movements of a pendulum system actuated by two antagonistic muscle-tendon complexes, addressing a tracking problem. The framework described in [19] involves the use of a pattern generator, the output of which is modulated by the trained neural model. This breakdown of the control problem, distinguishing baseline pattern generation and adjustments to the generated pattern, is reminiscent of some of the interplay between spinal structures (e.g. Central Pattern Generators, CPG, [20, 21]) and descending signals, which could prove helpful in investigating or emulating (for instance, in the aforementioned EES setting) such interactions. However, it remains unclear how effectively the neural model in [19] would generalize to more complex musculoskeletal systems or control tasks.

Improving performance of the control technology discussed in [8] and [9] could be pursued by exploiting available system information; that is, using model information, descriptive of the system acted upon (which includes in this case spinal circuitry and musculoskeletal system) to refine control action. This can be pursued by applying model-based control techniques ([22]). Such an avenue of investigation has been exploited, with for instance the application of backstepping techniques ([23]) to control muscle-actuated systems ([24-28]). In [24], the authors consider the actuation of a frictionless mass by a pair of antagonistic muscles. The approach provides interesting results, although it does not consider notions of cocontraction. Cocontraction constitutes a central paradigm of biological movement ([27-30]), intrinsic to muscle-driven actuation. A number of results have proposed the use of model predictive control addressing cocontraction, and more generally, aspects related to muscle

Raphael and Yannick are with the Dep. of Cog. Neuroscience, Fac. of Psych. and Neurosci., Maastricht University, Oxfordlaan 55, 6229EV Maastricht, Netherlands, {p.stolpe, y.morel}@maastrichtuniversity.nl.

This research has received funding from the European Union's Horizon 2020 Framework Programme for Research and Innovation under the Specific Grant Agreement No. 785907 (Human Brain Project SGA3).

redundancy ([31, 32]). For instance, in [31] the authors formulate cocontraction as an optimal control objective, resulting in well balanced muscle efforts. In [25] and [27], the authors investigate two connected open-chain linkages representative of the human arm, actuated by six pairwise antagonistic Hill-type muscles ([16, 33]). The authors construct a model-based controller using backstepping. The system being controlled features two Degrees of Freedom (DoF) representing mechanical joints, actuated by a redundant set of six muscles. Two different solutions are proposed to support the change of variable between (lower dimensional) joint space to (relatively higher dimensional) muscle space. In particular, the authors consider a least mean square solution to this change of variables (using the usual Moore-Penrose pseudoinverse, [34]). The approach results in unrealistically elevated tendon efforts ([27]). This behavior is compounded by the use of constant moment arms ([27]), which comes short of reflecting variations induced by changes in joint angle, as observed in physiology ([16]). Such an approximation has a substantial impact on the magnitude of torques generated. In an attempt to circumvent the issue, the authors resort to a minimization technique, considering a cost-function reflecting the magnitude of overall muscle activation. This results in more biologically plausible tendon forces (in spite of constant moment arms), but leads to non-smooth muscle length trajectories ([27]). In [25], the authors address the muscle redundancy problem using a comparable minimization technique, using a cost function designed to minimize efforts produced by muscle-tendon complexes. While both approaches provide convincing results, their reliance on optimization techniques, which may prove computationally expensive, complicates their application in real time.

In the following, we consider a class of musculoskeletal models featuring a set of antagonistic Hill-type muscles ([16, 33]). We design a model-based controller which, for the considered range of musculoskeletal models, produces muscle contraction signals supporting trajectory tracking in joint space, explicitly addressing aspects of cocontraction. The control approach is useful as a functional baseline to help investigate the type of functionality and signals necessary to support human-like motor control. The specific contribution of the presented result entails the provision of a guarantee of exponential stability of the origin of the constructed error system for the class of models considered, and the ability to directly adjust the magnitude of cocontraction across agonist and antagonist muscle pairs. In addition, the approach may be exploited to help inform EES signals, using a model descriptive of the considered patient. Special attention is afforded to the transition from joint space to muscle space, emphasizing reasonable, plausible muscle efforts.

This paper is structured as follows. Section II describes the class of musculoskeletal models considered. Section III outlines the proposed control approach. This approach is applied to an example of musculoskeletal model featuring two skeletal joints, actuated by five muscles. Results of numerical simulations are provided in Section IV. Section V concludes this paper.

II. Model Definition

In the following we consider movements of parts of a human skeletal system, in particular those of a given limb or set of limbs, under the effect of a set of muscle-tendon complexes. We assume the considered skeletal system is mechanically grounded and that bones composing this system behave as rigid segments. We further assume that joints between segments remain rotational in nature (i.e. revolute or ball joints). This is a limiting assumption, not allowing for instance to reflect kinematics of shoulder joints (see [35]), which will in the future be relaxed, but facilitates clarity of exposition. The state of the considered class of skeletal systems is described by a set of n joint angles $\theta(t) \in \mathcal{D}_\theta \subseteq \mathbb{R}^n$, $n \in \mathbb{N}$, $t \geqslant 0$, and angle velocities $\dot{\theta}(t) \in \mathbb{R}^n$. Its dynamics are described by the usual mechanical formulation,

$$M(\theta(t))\ddot{\theta}(t) + C(\theta(t), \dot{\theta}(t))\dot{\theta}(t) + g(\theta(t)) = \tau(t), \\ \theta(0) = \theta_0, \quad \dot{\theta}(0) = \dot{\theta}_0, \quad t \geqslant 0, \quad (1)$$

where the matrix $M(\cdot) \in \mathbb{R}^{n\times n}$ describes the system's inertia, $C(\cdot,\cdot) \in \mathbb{R}^{n\times n}$, $g(\cdot) \in \mathbb{R}^n$ represents the effect of gravity's acceleration, and $\tau(t) \in \mathbb{R}^n$ is the set of torques applied to the considered joints by relevant muscle-tendon complexes.

We describe the muscle dynamics using the model proposed in [16]. In particular, using the formulation in [16], we compute the torque vector in (1) as follows,

$$\tau(t) = \Omega(\theta(t))F\gamma_{\mathrm{s}}(\epsilon_{\mathrm{t}}(t)), \quad t \geqslant 0, \quad (2)$$

where the matrix $\Omega(\theta) \in \mathbb{R}^{n\times m}$ is rank n and describes the moment arms through which the $m \geqslant 2n$, $m \in \mathbb{N}$ considered muscle-tendon complexes generate torque, $\gamma_{\mathrm{s}}(\cdot) \in \mathbb{R}^{+m}$ represents the vector of normalized efforts produced by tendons as a result of tendon strains $\epsilon_{\mathrm{t}}(t) \in \mathbb{R}^{+m}$, and $F \in \mathbb{R}^{m\times m}$ is a diagonal matrix reflecting maximum isometric tendon forces. Tendon efforts are provided by the following equation,

$$\gamma_{\mathrm{s}i}(\epsilon_{\mathrm{t}i}) = \begin{cases} p_1\left(\mathrm{e}^{p_2\epsilon_{\mathrm{t}i}/\epsilon_{\mathrm{th}}} - 1\right) / \left(\mathrm{e}^{p_2} - 1\right), & \epsilon_{\mathrm{t}i} \leqslant \epsilon_{\mathrm{th}}, \\ p_3(\epsilon_{\mathrm{t}i} - \epsilon_{\mathrm{th}}) + p_1, & \epsilon_{\mathrm{t}i} > \epsilon_{\mathrm{th}}, \end{cases} \quad (3)$$

where $\gamma_{\mathrm{s}i} \in \mathbb{R}^+$ represents the i^{th} entry of γ_{s}, $i = 1, \ldots, m$, p_1, p_2, $p_3 \in \mathbb{R}^+$ are characteristic parameters, and $\epsilon_{\mathrm{th}} \in \mathbb{R}^+$ describes a threshold strain value. The tendon strains are computed as follows,

$$\epsilon_{\mathrm{t}i}(\theta, l_i) = \frac{\bar{l}_i(\theta) - l_i\cos(\alpha_i(l_i)) - l_{\mathrm{t}0i}}{l_{\mathrm{t}0i}}, \quad (4)$$

where $\bar{l}_i(\theta) \in \mathbb{R}^+$ describes the length of the i^{th} muscle-tendon complex, $l_i \in \mathbb{R}^+$ is the i^{th} muscle fiber's length, $l_{\mathrm{t}0i} \in \mathbb{R}^+$ is the i^{th} tendon's slack length, and the pennation angle $\alpha_i(l_i) \in \mathbb{R}^+$ is obtained from

$$\alpha_i(l_i) = \arccos\left(\sqrt{1 - \left(\frac{l_{\mathrm{r}i}\sin(\alpha_{\mathrm{r}i})}{l_i}\right)^2}\right), \quad (5)$$

where $l_{\mathrm{r}i} \in \mathbb{R}^+$ is a muscle fiber reference length. The muscle fiber length is obtained from the following nonlinear relationship,

$$\dot{l}(t) = h(\theta(t), l(t), q(t)), \quad l(0) = l_0, \quad t \geqslant 0, \quad (6)$$

where $q(t) \in (0, 1]^m$ represents the vector of normalized

muscle fiber contractions,

$$h_i(t) \triangleq \begin{cases} \frac{(\alpha_1+\alpha_2 q_i(t))(\gamma_{\mathrm{c}i}(t)-q_i(t)\gamma_{\mathrm{a}i}(t))}{q_i(t)\gamma_{\mathrm{a}i}(t)+\gamma_{\mathrm{c}i}(t)/\alpha_3}, & \gamma_{\mathrm{c}i}(t) \leqslant q_i(t)\gamma_{\mathrm{a}i}(t), \\ \frac{\alpha_4(\alpha_1+\alpha_2 q_i(t))(\gamma_{\mathrm{c}i}(t)-q_i(t)\gamma_{\mathrm{a}i}(t))}{\alpha_5 q_i(t)\gamma_{\mathrm{a}i}(t)+\gamma_{\mathrm{c}i}(t)}, & \gamma_{\mathrm{c}i}(t) > q_i(t)\gamma_{\mathrm{a}i}(t), \end{cases} \quad i = 1, \ldots, m, \quad (7)$$

where $h_i(t) \in \mathbb{R}$ represents the i^{th} entry of $h(t)$ in (6), $\alpha_j \in \mathbb{R}^+$, $j = 1, \ldots, 5$, are constant parameters, $q_i(t)$ represents the i^{th} entry of $q(t)$, and

$$\gamma_{\mathrm{p}i}(l_{\mathrm{n}i}) \triangleq \frac{\mathrm{e}^{(l_{\mathrm{n}i}-1)/\epsilon_{0\mathrm{m}}}-1}{\mathrm{e}^{k}-1}, \quad (8)$$

$$\gamma_{\mathrm{a}i}(l_{\mathrm{n}i}) \triangleq \mathrm{e}^{-(l_{\mathrm{n}i}-1)^2/g_{\mathrm{s}}}, \quad (9)$$

$$\gamma_{\mathrm{c}i}(\gamma_{\mathrm{s}i}, \gamma_{\mathrm{p}i}, \alpha_i) \triangleq \frac{\gamma_{\mathrm{s}i}}{\cos(\alpha_i)} - \gamma_{\mathrm{p}i}, \quad (10)$$

where $l_{\mathrm{n}i} \triangleq l_i/l_{ri}$ is the normalized i^{th} muscle length, k, $\epsilon_{0\mathrm{m}}$, $g_{\mathrm{s}} \in \mathbb{R}$ are constant parameters. The muscle activation vector $q(t) = \left[\begin{array}{ccc} q_1(t) & \ldots & q_m(t) \end{array}\right]^{\mathrm{T}}$ describes the signal produced by the nervous system to elicit muscle contractions. In the following we assume we are able to directly assign its rate of change, $\dot{q}(t)$, and design a control law such that the joint angles $\theta(t)$ are made to track a prescribed desired trajectory $\theta_{\mathrm{d}}(t) \in \mathbb{R}^n$.

III. Control Design

Consider the following joint angle and angular velocity errors,

$$e_1(t) \triangleq \theta_{\mathrm{d}}(t) - \theta(t), \quad t \geqslant 0, \quad (11)$$

$$e_2(t) \triangleq \dot{\theta}_{\mathrm{d}}(t) + G_1 e_1(t) - \dot{\theta}(t), \quad (12)$$

where $G_1 \in \mathbb{R}^{n\times n}$, $G_1 > 0$. Then define

$$\tau_{\mathrm{d}}(t) \triangleq C(\theta(t), \dot{\theta}(t))\dot{\theta}(t) + g(\theta(t)) + M(\theta(t))\Big(\ddot{\theta}_{\mathrm{d}}(t) + (I_n - G_1^2)e_1(t) + (G_1 + G_2)e_2(t)\Big), \quad (13)$$

where $I_n \in \mathbb{R}^{n\times n}$ represents the $n \times n$ identity, and $G_2 \in \mathbb{R}^{n\times n}$, $G_2 > 0$. Differentiating (11)–(12) in time, substituting in (1), and assuming that $\tau(t) \equiv \tau_{\mathrm{d}}(t)$, $t \geqslant 0$, we would obtain

$$\left[\begin{array}{c} \dot{e}_1(t) \\ \dot{e}_2(t) \end{array}\right] = \left[\begin{array}{cc} -G_1 & I_n \\ -I_n & -G_2 \end{array}\right] \left[\begin{array}{c} e_1(t) \\ e_2(t) \end{array}\right], \quad t \geqslant 0, \quad (14)$$

from which we would be able to straightforwardly conclude exponential convergence of the error vector $\left[\begin{array}{cc} e_1^{\mathrm{T}}(t) & e_2^{\mathrm{T}}(t) \end{array}\right]^{\mathrm{T}}$ to the origin.

We are not however able to directly define the torque profile $\tau(t)$, which instead is produced through action of the muscle-tendon complexes, as described by (2). In general, the system is overactuated, in that $m/2 > n$, where $m/2$ represents the number of effective agonistic-antagonistic muscle pairs. That is, a greater number of muscle pairs are made to act on a smaller number of joints. Accordingly, there exists no unique change of variable from joint space to muscle space. For instance, in light of (2), one could be tempted to define a desirable muscle effort profile as follows,

$$\gamma_{\mathrm{sd}}^*(t) \triangleq \left(\Omega(\theta(t))F\right)^{\dagger} \tau_{\mathrm{d}}(t), \quad t \geqslant 0, \quad (15)$$

where $\cdot^{\dagger}$ denotes the usual generalized inverse. This design choice would be similar to that adopted in [27, 28]. A possible issue emerging from such a choice relates to the nature of the normalized effort vector $\gamma_{\mathrm{s}}(t)$, the entries for which are in practice positive. However, there is no reason for the pseudo-inverse in (15) to result in consistently positive entries in the above-defined $\gamma_{\mathrm{sd}}^*(t)$. Attempting to track $\gamma_{\mathrm{sd}}^*(t)$ with $\gamma_{\mathrm{s}}(t)$ would therefore prove problematic. Instead, we carefully distinguish positive and negative parts of the entries in $\tau(t)$, thereby disentangling effort contributions from flexors and extensors. Specifically, consider

$$\tau_\mu(t) \triangleq \left[\begin{array}{c} \tau_{\mathrm{d}}^+(t) + c(\tau_{\mathrm{d}}(t)) \\ -\tau_{\mathrm{d}}^-(t) + c(\tau_{\mathrm{d}}(t)) \end{array}\right], \quad t \geqslant 0, \quad (16)$$

where $\tau_\mu \in \mathbb{R}^{2n}$, $\tau_{\mathrm{d}}^+(t) = \tau_{\mathrm{d}}(t)$ if $\tau_{\mathrm{d}}(t) > 0$, $\tau_{\mathrm{d}}^+(t) = 0$ otherwise, and $\tau_{\mathrm{d}}^-(t) = \tau_{\mathrm{d}}(t)$ if $\tau_{\mathrm{d}}(t) < 0$, $\tau_{\mathrm{d}}^-(t) = 0$ otherwise, and $c(\tau_{\mathrm{d}}(t)) \in \mathbb{R}^n$ is computed as follows,

$$c_i(\tau_{\mathrm{d}}(t)) \triangleq \frac{\mathrm{e}^{(-\alpha_s|\tau_{\mathrm{d}i}(t)|)}}{2\alpha_s} + \beta, \quad i = 1, \ldots, n, \quad (17)$$

where $c_i(t)$ is the i^{th} entry of vector $c(t)$, α_s, $\beta \in \mathbb{R}^+$. The vector $c(\cdot)$ is representative of cocontraction across flexors and extensors, and is designed in such a manner that $\tau_\mu(t)$ is continuously differentiable. Parameter α_s in (17) affects smoothness of $\tau_\mu(t)$, while β allows to adjust the magnitude of cocontraction. In practice, the net torques applied by the combination of flexors and extensors amounts to $\tau_{\mathrm{d}}^+(t) + \tau_{\mathrm{d}}^-(t) = \tau_{\mathrm{d}}(t)$, as the cocontraction terms $c(t)$ from flexors and extensors cancel out. More concretely, from (2), we are able to expand $\Omega(\theta(t))F$ to describe flexors and extensors contributions to joint torques as follows,

$$\left[\begin{array}{c} \tau^+(t) \\ \tau^-(t) \end{array}\right] = \Psi(\theta(t))\gamma_{\mathrm{s}}(\epsilon_{\mathrm{t}}(t)), \quad t \geqslant 0, \quad (18)$$

where $\tau^+(t)$, $\tau^-(t) \in \mathbb{R}^n$ represent torque produced by flexors and extensors, and $\Psi(\theta(t)) \in \mathbb{R}^{2n\times m}$ describes a change of coordinates from muscle space to torque space, allowing to map contributions from flexors and extensors onto the actuated joints. Provided that the considered set of muscle-tendon complexes provides sufficient control authority over the considered joints, one is always able to construct one such mapping (see illustrative application in Section IV, (42)). Then, define

$$\gamma_{\mathrm{sd}}(t) \triangleq \Psi^{\dagger}(\theta(t))\tau_\mu(t), \quad (19)$$

which is such that if $\gamma_{\mathrm{s}}(t) \equiv \gamma_{\mathrm{sd}}(t)$, $t \geqslant 0$, then $\tau(t) \equiv \tau_{\mathrm{d}}(t)$, $t \geqslant 0$, and (14) is verified. Accordingly, define

$$e_3(t) \triangleq \gamma_{\mathrm{sd}}(t) - \gamma_{\mathrm{s}}(t), \quad t \geqslant 0, \quad (20)$$

$$e_4(t) \triangleq \dot{l}_{\mathrm{d}}(t) - \dot{l}(t), \quad (21)$$

where $\gamma_{\mathrm{sd}}(t)$ is provided by (19) and

$$\dot{l}_{\mathrm{d}}(t) \triangleq \left(\frac{\partial \gamma_{\mathrm{s}}(t)}{\partial l(t)}\right)^{-1} \Big(-\frac{\partial \gamma_{\mathrm{s}}(t)}{\partial \theta(t)}\dot{\theta}(t) + \Gamma^{\mathrm{T}}(\theta(t))e_2(t) + \dot{\gamma}_{\mathrm{sd}}(t) + G_3 e_3(t)\Big), \quad t \geqslant 0, \quad (22)$$

where $G_3 \in \mathbb{R}^{m\times m}$, $G_3 > 0$, and $\Gamma(\theta) \triangleq M^{-1}(\theta)\Omega(\theta)F$. For brevity, we do not provide the closed-form expressions from which one may compute $\partial\gamma_{\mathrm{s}}(t)/\partial l(t)$, $\partial\gamma_{\mathrm{s}}(t)/\partial\theta(t)$, $\dot{\gamma}_{\mathrm{sd}}(t)$, they can be straightforwardly obtained from (3)–(5) and (19). The desired muscle fiber velocity (22) was designed, together with the desired torque (13) using a backstepping procedure ([23]). In the following, we build

upon this set of tracking errors to pursue convergence of the joint angles $\theta(t)$ to their desired trajectories $\theta_{\rm d}(t)$.

Theorem 1: Consider the joint angle trajectory $\theta(t)$, $t \geqslant 0$, produced by the musculoskeletal system composed of (1) and (6), its desired trajectory $\theta_{\rm d}(t)$, and the following choice of muscle fiber activation rate,

$$\dot{q}(t) = \left(\frac{\partial h(t)}{\partial q(t)}\right)^{-1} \left(G_4 e_4(t) - \frac{\partial h(t)}{\partial \theta(t)}\dot{\theta}(t) - \frac{\partial h(t)}{\partial l(t)} h(t) + \left(\frac{\partial \gamma_{\rm s}(t)}{\partial l(t)}\right)^{\rm T} e_3(t) + \ddot{l}_{\rm d}(t) \right), \; q(0) = q_0, \; t \geqslant 0, \quad (23)$$

where $G_4 \in \mathbb{R}^{m\times m}$, $G_4 > 0$, $h(t)$ is given by (7), tracking errors $e_3(t)$ and $e_4(t)$ are provided by (20), (21), the normalized series elastic force $\gamma_{\rm s}(t)$ is provided by (3), and $\ddot{l}_{\rm d}(t)$ is obtained by differentiating over time the desired muscle fiber speed (22).

Using the muscle fiber activation $q(t)$ obtained from (23) as input to model (1), (6), guarantees exponential convergence of $\theta(t)$ to $\theta_{\rm d}(t)$.

Proof: Differentiating (11) over time along the trajectories of the system composed of (1) and (6) subjected to the control input $q(t)$ obtained from (23), substituting in (12) leads to

$$\dot{e}_1(t) = -G_1 e_1(t) + e_2(t), \quad t \geqslant 0. \quad (24)$$

Similarly, from (12), (20), (1), (13), (16), and (19), we obtain

$$\dot{e}_2(t) = -e_1(t) - G_2 e_2(t) + \Gamma(\theta(t)) e_3(t). \quad (25)$$

From (20), (21), (6), and (22), we have

$$\dot{e}_3(t) = -\Gamma^{\rm T}(\theta(t)) e_2(t) - G_3 e_3(t) + \frac{\partial \gamma_{\rm s}(t)}{\partial l(t)} e_4(t). \quad (26)$$

Finally, differentiating (21) and substituting in (23) yields

$$\dot{e}_4(t) = -\left(\frac{\partial \gamma_{\rm s}(t)}{\partial l(t)}\right)^{\rm T} e_3(t) - G_4 e_4(t). \quad (27)$$

Define $e(t) \triangleq \left[\begin{array}{cccc} e_1^{\rm T}(t) & e_2^{\rm T}(t) & e_3^{\rm T}(t) & e_4^{\rm T}(t) \end{array}\right]^{\rm T}$, $t \geqslant 0$. From (24)–(27), we have

$$\dot{e}(t) = \bar{A}(\theta(t), l(t))\, e(t), \quad (28)$$

where

$$\bar{A}(\theta, l) \triangleq \left[\begin{array}{cccc} -G_1 & I_n & 0_{n\times m} & 0_{n\times m} \\ -I_n & -G_2 & \Gamma(\theta) & 0_{n\times m} \\ 0_{m\times n} & -\Gamma^{\rm T}(\theta) & -G_3 & \frac{\partial \gamma_{\rm s}(\theta,l)}{\partial l} \\ 0_{m\times n} & 0_{m\times n} & -(\frac{\partial \gamma_{\rm s}(\theta,l)}{\partial l})^{\rm T} & -G_4 \end{array}\right], \quad (29)$$

where $0_{i\times j}$ denotes the $i \times j$ zero matrix.

Then, consider the error system consisting of (28) with initial condition $e(0) = e_0$, and the following Lyapunov candidate for this system,

$$V(e) \triangleq \frac{1}{2} e^{\rm T} e. \quad (30)$$

Differentiating (30) along the trajectories of the considered error system provides

$$\begin{aligned} \dot{V}(e(t)) &= e^{\rm T}(t) \bar{A}(\theta(t), l(t)) e(t), \quad t \geqslant 0, \\ &= -e^{\rm T}(t) G e(t), \end{aligned} \quad (31)$$

where $G \triangleq \operatorname{diag}\left(\left[\begin{array}{cccc} G_1 & G_2 & G_3 & G_4 \end{array}\right]\right)$. From (30), we have that $k_1 \|e\|^2 \leqslant V(e) \leqslant k_2 \|e\|^2$ with $k_1 = k_2 = 1/2$. From (31), we have that $\dot{V}(e(t)) \leqslant -k_3 \|e(t)\|^2$ with $k_3 \triangleq \lambda_{\min}(G)$ strictly positive by construction of G. It follows ([36]) that the origin is an exponentially stable equilibrium point of the error system. From (11), it directly follows that $\theta(t)$ converges to $\theta_{\rm d}(t)$, exponentially. ■

Note that the control designer is able to adjust control gains G_i, $i = 1, \ldots, 4$, to adjust stiffness of the error system's response to prescribed desired trajectories. In particular, mechanical impedance of the response may be adjusted through selection of G_1, G_2. Efficacy of the result in Theorem 1 can be verified through numerical simulation, as presented in Section IV. However, for a meaningful range of musculoskeletal models, the error state matrix $\bar{A}(\theta, l)$ in (29) is characterized by strong oscillatory modes. Existence of these modes, the emergence of which can be traced to large values in $\Gamma(\theta)$ and $\partial \gamma_{\rm s}(\theta, l)/\partial l$, affects closed-loop behavior of the system in an undesirable manner. In particular, initial errors may lead to excessive and brutal oscillations in the transient. To mitigate the issue, we propose a minor adjustment to the above result.

This adjustment amounts to omitting compensating cross terms in the desired muscle fiber velocity (22) and contraction rate (23). Specifically, consider the following alternate desired fiber velocity,

$$\dot{l}_{\rm d}(t) = \left(\frac{\partial \gamma_{\rm s}(t)}{\partial l(t)}\right)^{-1} \Big(-\frac{\partial \gamma_{\rm s}(t)}{\partial \theta(t)}\dot{\theta}(t) + \dot{\gamma}_{\rm sd}(t) + G_3 e_3(t) \Big), \quad t \geqslant 0. \quad (32)$$

Omitting in (32) the term $\Gamma^{\rm T}(\theta) e_2$, originally present in (22), will lead to the emergence of an additional, undesirable term in the Lyapunov derivative. With a particular choice of control gains, we are able to overcome the negative influence of this perturbing term, helping to circumvent the emergence of undesirable oscillatory modes without jeopardizing stability of the solution of the error system, as stated in the following. For ease of exposition, let

$$\Lambda(\theta, l) \triangleq \left[\begin{array}{ccc} 0_{n\times 2n} & 0_{n\times m} & 0_{n\times m} \\ 0_{n\times 2n} & \Gamma(\theta) & 0_{n\times m} \\ 0_{m\times 2n} & 0_{m\times m} & \frac{\partial \gamma_{\rm s}(\theta,l)}{\partial l} \\ 0_{m\times 2n} & 0_{m\times m} & 0_{m\times m} \end{array}\right]. \quad (33)$$

Theorem 2: Consider the joint angle trajectory $\theta(t)$, $t \geqslant 0$, produced by the musculoskeletal system composed of (1) and (6), consider the desired trajectory $\theta_{\rm d}(t)$, and the following choice of muscle fiber activation rate,

$$\dot{q}(t) = \left(\frac{\partial h(t)}{\partial q(t)}\right)^{-1} \Big(G_4 e_4(t) - \frac{\partial h(t)}{\partial \theta(t)}\dot{\theta}(t) - \frac{\partial h(t)}{\partial l(t)} h(t) + \ddot{l}_{\rm d}(t) \Big), \quad q(0) = q_0, \quad t \geqslant 0, \quad (34)$$

where $G_4 \in \mathbb{R}^{m\times m}$, $G_4 > 0$, $h(t)$ is given by (7), tracking errors $e_3(t)$ and $e_4(t)$ are provided by (20), (21), the normalized series elastic force $\gamma_{\rm s}(t)$ is provided by (3), and $\ddot{l}_{\rm d}(t)$ is obtained by differentiating over time the adjusted desired muscle fiber speed (32). In addition, select the control gains G_i, $i = 1, \ldots, 4$, in (13), (32), and (34) such that $\lambda_{\min}(G_2) > 1$, $\lambda_{\min}(G_3) > \lambda_{\max}(I_m + \Gamma^{\rm T}(t)\Gamma(t)/4)$

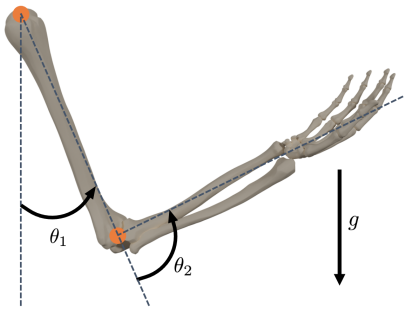

Fig. 1: Skeletal system and joint angle definitions.

uniformly in time, and $\lambda_{\min}(G_4) > \lambda_{\max}(\rho^{\mathrm{T}}(t)\rho(t)/4)$ uniformly in time, where $\rho(t) \triangleq \partial\gamma_{\mathrm{s}}(t)/\partial l(t)$. Using the muscle fiber activation $q(t)$ obtained from (34) as input to model (1), (6), guarantees exponential convergence of $\theta(t)$ to $\theta_{\mathrm{d}}(t)$.

Proof: The modified desired fiber speed (32) and activation rate (34) lead to the following error dynamics,

$$\dot{e}(t) = A(\theta(t), l(t))\, e(t), \quad t \geqslant 0, \tag{35}$$

with

$$A(\theta, l) \triangleq \begin{bmatrix} -G_1 & I_n & 0_{n\times m} & 0_{n\times m} \\ -I_n & -G_2 & \Gamma(\theta) & 0_{n\times m} \\ 0_{m\times n} & 0_{m\times n} & -G_3 & \rho(\theta, l) \\ 0_{m\times n} & 0_{m\times n} & 0_{m\times m} & -G_4 \end{bmatrix}. \tag{36}$$

Using the same Lyapunov candidate (30), differentiating it over time along the trajectories of this new closed-loop system, we obtain

$$\begin{aligned} \dot{V}(t) &= -e^{\mathrm{T}}(t)Ge(t) + e^{\mathrm{T}}(t)\Lambda(t)e(t), \\ &= -e^{\mathrm{T}}(t)Ge(t) + e_2^{\mathrm{T}}(t)\Gamma(t)e_3(t) + e_3^{\mathrm{T}}(t)\rho(t)e_4(t). \end{aligned}$$

Completing the squares, we obtain

$$\begin{aligned} \dot{V}(t) = &-e^{\mathrm{T}}(t)Ge(t) + e_2^{\mathrm{T}}(t)e_2(t) + e_3^{\mathrm{T}}(t)e_3(t) \\ &-(e_2(t) - \Gamma(t)e_3(t)/2)^{\mathrm{T}}(e_2(t) - \Gamma(t)e_3(t)/2) \\ &-(e_3(t) - \rho(t)e_4(t)/2)^{\mathrm{T}}(e_3(t) - \rho(t)e_4(t)/2) \\ &+e_3^{\mathrm{T}}(t)\Gamma^{\mathrm{T}}(t)\Gamma(t)e_3(t)/4 + e_4^{\mathrm{T}}(t)\rho^{\mathrm{T}}(t)\rho(t)e_4(t)/4, \\ \leqslant &-\lambda_{\min}(G_1)\|e_1(t)\|^2 - (\lambda_{\min}(G_2) - 1)\|e_2(t)\|^2 \\ &-(\lambda_{\min}(G_3) - \lambda_{\max}(I_m + \Gamma^{\mathrm{T}}(t)\Gamma(t)/4))\|e_3(t)\|^2 \\ &-(\lambda_{\min}(G_4) - \lambda_{\max}(\rho^{\mathrm{T}}(t)\rho(t)/4))\|e_4(t)\|^2. \end{aligned} \tag{37}$$

By construction of G_i, $i = 2, 3, 4$, there exist $r_i \in \mathbb{R}^{+*}$ such that $r_2 < \lambda_{\min}(G_2) - 1$, $r_3 < \lambda_{\min}(G_3) - \lambda_{\max}(I_m + \Gamma^{\mathrm{T}}(t)\Gamma(t)/4)$, $r_4 < \lambda_{\min}(G_4) - \lambda_{\max}(\rho^{\mathrm{T}}(t)\rho(t)/4)$.

Then, let $k_4 \triangleq \min\{\lambda_{\min}(G_1), r_2, r_3, r_4\}$. It follows from (37) that $\dot{V}(e(t)) \leqslant -k_4\|e(t)\|^2$ with k_4 strictly positive. In addition, from (30), we have $(1/2)\|e\|^2 \leqslant V(e) \leqslant (1/2)\|e\|^2$. Accordingly, the origin is an exponentially stable equilibrium point of the modified error system, and $\theta(t) \to \theta_{\mathrm{d}}(t)$ as $t \to \infty$, exponentially. ■

This Section has proposed two distinct control designs addressing the tracking control problem for a class of musculoskeletal systems. In the following Section, we apply these designs to an example and present results of numerical simulations, illustrating their respective merits.

IV. Illustrative Application

We consider a two DoF skeletal system ($n = 2$), actuated by a set of five muscle-tendon complexes ($m = 5$). This musculoskeletal model represents an approximation of an upper limb, with DoFs representing a rotational joint in the shoulder and in the elbow. See Figure 1 for an illustration of the skeletal system and sign definition of the considered joint angles. Specifically, the humerus is connected to the torso through the shoulder joint, represented using a rotational joint (described by $\theta_1(t)$, $t \geqslant 0$). Ulna and radius are together connected to the humerus through the elbow joint, which is also here approximated as a single DoF rotational joint ($\theta_2(t)$). Two of the muscle-tendon complexes are flexors, three are extensors one of which is biarticular. The Anterior Deltoid acts as a flexor on the shoulder joint, whereas the Triceps long acts antagonistically on the shoulder joint. The Triceps long head is biarticular and, in combination with the Triceps medial and lateral, acts as extensor on the elbow joint. Lastly, Brachialis is a flexor of the elbow joint.

For the purpose of numerical simulation, we use a mass of $m_1 = 1.86$kg for the humerus, $m_2 = 1.53$kg for the combined ulna and radius, and respective lengths of $l_1 = 0.29$m and $l_2 = 0.24$m (values taken from [37]). Each segment is approximated as a thin rod of uniform mass density. The maximal isometric tendon forces, reference muscle lengths, tendon slack lengths, and reference pennation angles for each of the five considered muscles are provided in Table 1 (values adapted from [38]). Numerical integration is done using `ode45` ([39]).

To illustrate performance of the control laws presented in Section III, we simulate tracking of a sinusoidal trajectory $\theta_{\mathrm{d}}(t) = a\sin(\omega t + \phi) + b$, $t \geqslant 0$, where $a = \pi/180\ \mathrm{diag}\left(\begin{bmatrix} 45 & 11.25 \end{bmatrix}\right)$rad, $\omega = \begin{bmatrix} 3/\pi & 4/\pi \end{bmatrix}^{\mathrm{T}}$rad/s, $\phi = \begin{bmatrix} 0 & 0 \end{bmatrix}^{\mathrm{T}}$rad, and $b = \pi/180 \begin{bmatrix} 67.5 & 22.5 \end{bmatrix}^{\mathrm{T}}$rad. Values of the control gains are $G_1 = 5\,I_n$, $G_2 = 2\,I_n$, $G_3 = 500\,I_m$ and $G_4 = 500\,I_m$ when applying the control defined in (23), and $G_1 = 5\,I_n$, $G_2 = 2\,I_n$, $G_3(t) = 20\,I_m$ and $G_4(t) = 20\,I_m$ for that in (34). $M(\theta)$, $C(\theta, \dot{\theta})$ and $g(\theta)$ are of the form

$$M(\theta) = \begin{bmatrix} 1 & \frac{l_2 m_2}{l_1(m_1+m_2)}\cos(\theta_1 - \theta_2) \\ \frac{l_1}{l_2}\cos(\theta_1 - \theta_2) & 1 \end{bmatrix}, \tag{38}$$

$$C(\theta, \dot{\theta}) = \begin{bmatrix} 0 & \frac{l_2 m_2}{l_1(m_1+m_2)}\sin(\theta_1 - \theta_2)\dot{\theta}_2 \\ -\frac{l_1}{l_2}\sin(\theta_1 - \theta_2)\dot{\theta}_1 & 0 \end{bmatrix}, \tag{39}$$

$$g(\theta) = \begin{bmatrix} \frac{g}{l_1}\sin(\theta_1) & \frac{g}{l_2}\sin(\theta_2) \end{bmatrix}^{\mathrm{T}}, \tag{40}$$

where $g = 9.81\mathrm{m/s}^2$. $\Omega(\theta)$ in (2) is of the form

$$\Omega(\theta) = \begin{bmatrix} \omega_{11}(\theta_1) & \omega_{12}(\theta_1) & 0 & 0 & 0 \\ 0 & \omega_{22}(\theta_2) & \omega_{23}(\theta_2) & \omega_{24}(\theta_2) & \omega_{25}(\theta_2) \end{bmatrix}, \tag{41}$$

Muscle	F [N]	l_r [cm]	l_{t0} [cm]	α_{r} [deg]
Anterior Deltoid (DELT1)	1,218.9	9.76	9.3	22
Triceps long head (TRIlong)	501.7	13.4	14.3	12
Triceps lateral (TRIlat)	609.9	11.38	9.8	9
Triceps medial (TRImed)	932.7	11.38	9.08	9
Brachialis (BRA)	4,120.8	8.58	5.35	0

Tab. 1: Muscle-Tendon Parameters

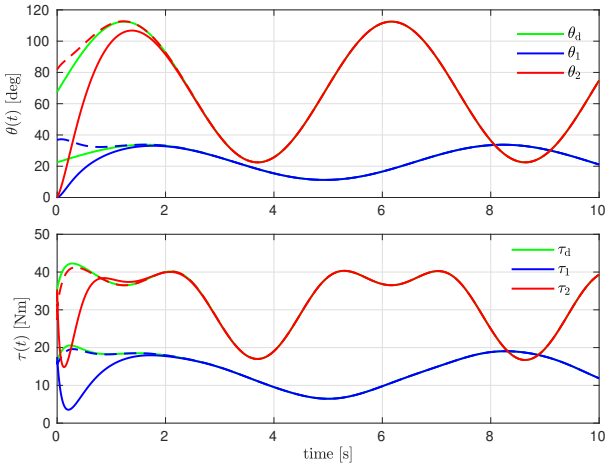

Fig. 2: Desired (green) and actual joint angle trajectories (shoulder joint in blue, elbow in red, Theorem 1 dashed, Theorem 2 solid, top), desired and actual torques (bottom).

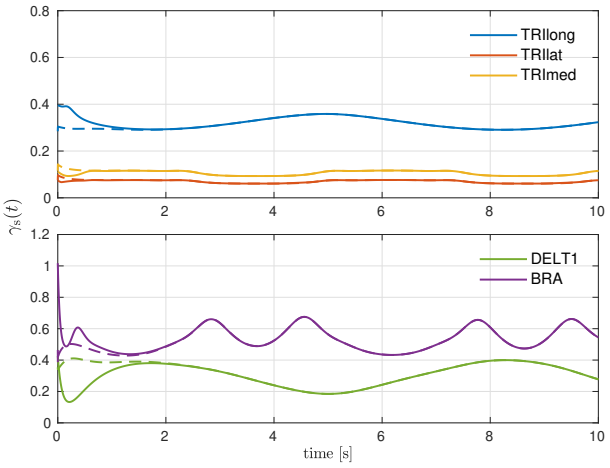

Fig. 3: Normalized tendon efforts for extensors TRIlong, TRIlat, TRImed (top), and flexors DELT1, BRA (bottom), result from Theorem 1 shown in dashed, Theorem 2 solid.

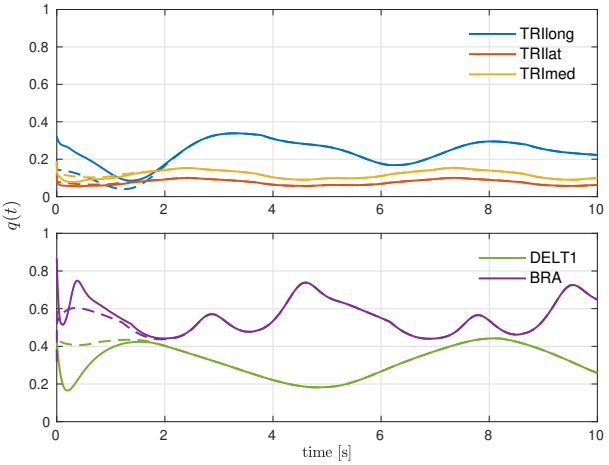

Fig. 4: Muscle fibar activation for extensors TRIlong, TRIlat, TRImed (top) and flexors DELT1, BRA (bottom), result obtained from Theorem 1 shown in dashed, Theorem 2 solid.

where the specific expressions of ω_{ij}, $i = 1, 2$, $j = 1, \ldots, 5$, are provided by [40]. The specific values used in (3) and (7-9) are taken from [37] (which itself is adapted from [16]); $p_1 = 0.33$, $p_2 = 51.8749$, $p_3 = 3$, $\epsilon_{\text{th}} = 0.0201$, $\alpha_1 = 1/4$, $\alpha_2 = 3/4$, $\alpha_3 = 3/10$, $\alpha_4 = 0.0923$, $\alpha_5 = 1.8$, $e_{0\text{m}} = 6/10$, $k = 4$ and $g = 1/2$. In addition, we select $\alpha_s = 0.5$, $\beta = 3$, and the muscle recruitment matrix is of the form

$$\Psi(\theta) = \begin{bmatrix} \psi_{11}(\theta_1) & 0 & 0 & 0 & 0 \\ 0 & \psi_{22}(\theta_1,\theta_2) & 0 & 0 & 0 \\ 0 & 0 & 0 & 0 & \psi_{35}(\theta_2) \\ 0 & \psi_{42}(\theta_1,\theta_2) & \psi_{43}(\theta_2) & \psi_{44}(\theta_2) & 0 \end{bmatrix}, \quad (42)$$

where the specific values of ψ_{ij} are directly derived from entries of $\Omega(\theta)$. Values for $\bar{l}(\theta)$ are taken from [38]. Tracking performance is shown in Figure 2. Initial conditions used when applying the result from Theorem 1 are the following, $\theta_0 = \begin{bmatrix} 0.6427 & 1.4281 \end{bmatrix}^{\text{T}}$rad, $\dot{\theta}_0 = \dot{\theta}_{\text{d}}(0)$, $l_0 = \begin{bmatrix} 8.83 & 17.97 & 10.08 & 9.57 & 7.07 \end{bmatrix}^{\text{T}}$cm and $q_0 = \begin{bmatrix} 0.3323 & 0.1866 & 0.1240 & 0.1898 & 0.3175 \end{bmatrix}^{\text{T}}$. For the result from Theorem 2, we used $\theta_0 = \begin{bmatrix} 0 & 0 \end{bmatrix}^{\text{T}}$rad, $\dot{\theta}_0 = \dot{\theta}_{\text{d}}(0)$, $l_0 = \begin{bmatrix} 11.36 & 13.60 & 6.93 & 6.43 & 8.76 \end{bmatrix}^{\text{T}}$cm and $q_0 = \begin{bmatrix} 0.2498 & 0.3233 & 0.0764 & 0.1302 & 0.5409 \end{bmatrix}^{\text{T}}$. Tracking performance is excellent. Initial conditions used to simulate the closed-loop using the control law from Theorem 1 were selected to avoid excessive transient oscillations, as discussed in Section III. This constraint is relaxed when using the controller presented in Theorem 2, as illustrated in Figure 2. Upon reaching steady state (from about $t = 2$s), trajectories appear consistent across both control laws. Normalized tendon efforts for extensors and flexors are shown in Figure 3 (top and bottom, respectively), the corresponding muscle fiber activations in Figure 4. Note that by definition of $q(t)$, activation values are expected to remain within $(0, 1]$. Here, ensuring that activation remains positive can be achieved by adjusting the cocontraction parameter β in (17). Avoiding that activation exceeds its maximal value is achieved by selecting achievable (given initial conditions and model parameters, in particular F) desired trajectories. Alternatively, one may employ actuation saturation techniques such as that in [41].

V. Conclusion

The work presented addresses the tracking problem for a class of musculoskeletal systems. Results provided achieve exponential convergence of skeletal joint angles to user-defined desired angle trajectories. Application to a two DoF model of an upper limb, actuated by a set of five muscles, is provided to illustrate performance of the control laws. Future work will address a number of different aspects. In particular, steps are being taken to provide the approach with a measure of robustness to system uncertainty, using adaptive and robust control techniques, such as that in [42], which has in the past been applied to a robotic model of a swimmer ([43]). Similarly, the output feedback problem will be addressed to more closely reflect the type of control problem solved by the nervous system, in particular considering feedback from muscle spindles (as is the case in biology) in the stead of assuming direct availability of muscle fiber length. In

addition, the considered system will be extended to include a functional spinal cord model. At that stage, the control law will act at the level of descending signals ([44, 45]). The setup will be used to investigate the contribution to closed-loop behavior of different spinal pathways, allowing to interrogate and assess merit of existing models of such pathways proposed in the computational neuroscience literature. In the longer term, this avenue of investigation will be exploited to support functional dynamical grounding of detailed neural sensorimotor loop models, with applications to digital modeling of patients suffering from adverse motor conditions (e.g. post-stroke paresis). Such models (i.e. neurophysical digital twins [46]) can be used to help inform physical therapies relied upon to help improve patients' condition.

REFERENCES

[1] G. Rizzolatti and G. Luppino, 'The cortical motor system', Neuron, vol. 31, no. 6, pp. 889–901, Sep. 2001.

[2] E. Pierrot-Deseilligny and D. Burke, 'The circuitry of the human spinal cord: Its role in motor control and movement disorders', Cambridge University Press, 2005.

[3] F. Filimon, 'Human cortical control of hand movements: Parietofrontal networks for reaching, grasping, and pointing', Neuroscientist, vol. 16, no. 4, pp. 388–407, Aug. 2010.

[4] T. J. Prescott, et al., 'Embodied Models and Neurorobotics', MIT Press, pp. 483–512, 2016.

[5] H. E. Matheson and L. W. Barsalou, 'Embodiment and Grounding in Cognitive Neuroscience', in Stevens' Handb. of Exp. Psych. and Cog. Neurosci., John Wiley & Sons, pp. 1–27, 2018.

[6] B. Feldotto, F. O. Morin, and A. Knoll. 'The Neurorobotics Platform Robot Designer: Modeling Morphologies for Embodied Learning Experiments', Frontiers in Neurorobotics 16, 2022.

[7] M. Senden, J. Peters, F. Röhrbein, G. Deco, and R. Goebel. 'The Embodied Brain: Computational Mechanisms of Integrated Sensorimotor Interactions With a Dynamic Environment', Frontiers in Computational Neuroscience 14, 2020.

[8] F. B. Wagner et al., 'Targeted neurotechnology restores walking in humans with spinal cord injury', Nature 2018, vol. 563, no. 7729, pp. 65–71, Oct. 2018.

[9] A. Rowald et al., 'Activity-dependent spinal cord neuromodulation rapidly restores trunk and leg motor functions after complete paralysis', Nat. Med., vol. 28, no. 2, Feb. 2022.

[10] S. Yakovenko, et al., 'Spatiotemporal Activation of Lumbosacral Motoneurons in the Locomotor Step Cycle', Journal of Neurophysiology, vol. 87, no. 3, pp. 1542–1553, Mar. 2002.

[11] N. Wenger et al., 'Closed-loop neuromodulation of spinal sensorimotor circuits controls refined locomotion after complete spinal cord injury', Sci. Transl. Med., vol. 6, no. 255, Sep. 2014.

[12] N. Wenger et al., 'Spatiotemporal neuromodulation therapies engaging muscle synergies improve motor control after spinal cord injury', Nat. Med., vol. 22, no. 2, pp. 138–145, Feb. 2016.

[13] M. Capogrosso et al., 'Configuration of electrical spinal cord stimulation through real-time processing of gait kinematics', Nat. Protoc., vol. 13, no. 9, pp. 2031–2061, Sep. 2018.

[14] M. Ferrarin, et al., 'An experimental PID controller for knee movement restoration with closed loop FES system', in Proc. of 18th Ann. Int. Conf. of the IEEE Eng. in Med. and Biol. Soc., vol. 1, pp. 453–454, Oct. 1996.

[15] K. Jagodnik and A. van den Bogert, 'Optimization and Evaluation of a Proportional Derivative Controller for Planar Arm Movement', Journal of Biomechanics, vol. 43, no. 6, pp. 1086–1091, Apr. 2010.

[16] D. G. Thelen, 'Adjustment of Muscle Mechanics Model Parameters to Simulate Dynamic Contractions in Older Adults', Journal of Biomechanical Engineering, vol. 125, no. 1, pp. 70–77, Feb. 2003.

[17] J. Houk, et al., 'Resp. of Golgi tendon organs to forces applied to muscle tendon', Journal of Neurophys. 30, no. 6, pp. 1466-1481, 1967.

[18] M. Hayashibe, P. Poignet, D. Guiraud, and H. El Makssoud, 'Nonlinear identification of skeletal muscle dynamics with sigma-point Kalman filter for model-based FES', In 2008 IEEE International Conf. on Robotics and Automation, pp. 2049-2054. IEEE, 2008.

[19] J. J. Abbas and H. J. Chizeck, 'Neural network control of functional neuromuscular stimulation sys.: computer simulation studies', IEEE Trans. on Biom. Eng., vol. 42, no. 11, pp. 1117–1127, Nov. 1995.

[20] A. J. Ijspeert, 'Central pattern generators for locomotion control in animals and robots: A review', Neural Networks, vol. 21, no. 4, pp. 642–653, May 2008.

[21] S. Grillner, and P. Wallen, 'Central pattern generators for locomotion, with special reference to vertebrates', Annual review of neuroscience, vol. 8, no. 1, pp. 233-261, 1985.

[22] C. Brosilow, and B. Joseph, 'Techniques of model-based control', Prentice Hall Professional, 2002.

[23] M. Krstic, I. Kanellakopoullos, and P. Kokotovic, 'Nonlinear and Adaptive Control Design', John Wiley & Sons, 1995.

[24] B. Koo and A. Leonessa, 'An Adaptive Block Backstepping Control Design for Functional Electrical Stimulation of Agonist-Antagonist Muscles', in Dyn. Sys. and Control Conf., pp. 479–486, May 2012.

[25] C.H. Nguyen and A. Leonessa, 'Control Motion of a Human Arm: A Simulation Study', In International Conf. of Control, Dynamic Systems, and Robotics, May 2014.

[26] H. Warner, H. Richter, and A. van den Bogert, 'Nonlinear Tracking Control of an Antagonistic Muscle Pair Actuated System', presented at the ASME 2017 Dyn. Sys. and Control Conf., Nov. 2017.

[27] H. Warner et al., 'Backstepping Control of Open-Chain Linkages Actuated by Antagonistic Hill Muscles', Journal of Dyn. Sys., Measurement, and Control, vol. 142, no. 10, Jun. 2020.

[28] H. De las Casas and H. Richter, 'Backstepping Control of Muscle Driven Systems with Redundancy Resolution', arXiv e-prints, 2020.

[29] P. L. Gribble, et al., 'Role of cocontraction in arm movement accuracy', Journ. of Neurophys., vol. 89, no. 5, pp. 2396-2405, 2003.

[30] M. Darainy and D. J. Ostry, 'Muscle cocontraction following dynamics learning', Exp. Brain Research, vol. 190, no. 2, pp. 153-163, 2008.

[31] H. Richter and H. Warner, 'Motion Optimization for Musculoskeletal Dynamics: A Flatness-Based Polynomial Approach', IEEE TAC, 2021.

[32] F. Towhidkhah, R. E. Gander, and H. C. Wood, 'Model Predictive Impedance Control: A Model for Joint Movement', Journal of Motor Behavior, vol. 29, no. 3, pp. 209–222, Sep. 1997.

[33] A. V. Hill, 'The heat of shortening and the dynamic constants of muscle', Proceedings of the Royal Society of London. Series B - Biological Sciences, vol. 126, no. 843, pp. 136–195, Oct. 1938.

[34] R. Penrose, 'A generalized inverse for matrices', Mathematical Proceedings of the Cambridge Philosophical Society, vol. 51, pp. 406–413. 1955.

[35] D. B. Lucas, 'Biomechanics of the Shoulder Joint', Archives of Surgery, vol. 107, no. 3, pp. 425–432, Sep. 1973.

[36] H. K. Khalil, 'Nonlinear Systems', Upper Saddle River, NJ: Prentice Hall, third ed., 2002.

[37] S. L. Delp et al., 'OpenSim: Open-source software to create and analyze dynamic simulations of movement', IEEE Transactions on Biomedical Engineering, vol. 54, no. 11, pp. 1940–1950, Nov. 2007.

[38] K. R. S. Holzbaur, W. M. Murray, and S. L. Delp, 'A model of the upper extremity for simulating musculoskeletal surgery and analyzing neuromuscular control', Annals of biomed. Eng., vol. 33, no. 6, pp. 829–840, Jun. 2005.

[39] J. R. Dormand and P. J. Prince, 'A family of embedded Runge-Kutta formulae', Journal of Computational and Applied Mathematics, vol. 6, no. 1, pp. 19–26, Mar. 1980.

[40] M. A. Sherman, et al., 'What is a Moment Arm? Calculating Muscle Effectiveness in Biomechanical Models Using Generalized Coordinates', ASME 2013 Intern. Design Eng. Techn. Conf.s and Computers and Information in Eng. Conf., Feb. 2014.

[41] Leonessa, A., et al., 'Adaptive Control for Nonlinear Uncertain Systems with Actuator Amplitude and Rate Saturation Constraints', Int. Journal of Adapt. Control and Signal Proceedings, vol. 23, no. 1, pp. 73–96, 2009.

[42] Y. Morel and A. Leonessa., 'Nonlinear predictor-based output feedback control for a class of uncertain nonlinear systems', In Dynamic Systems and Control Conf., pp. 939-946. 2010.

[43] Y. Morel, M. Porez, A. Leonessa, and A. J. Ijspeert., 'Nonlinear motion control of CPG-based movement with applications to a class of swimming robots', In 2011 50th IEEE Conf. on Decision and Control and European Control Conf., pp. 6331-6336. IEEE, 2011.

[44] S. Grillner and A. El Manira, 'Current Principles of Motor Control, with Special Reference to Vertebrate Locomotion', Physiological Reviews, vol. 100, no. 1, pp. 271–320, Jan. 2020.

[45] R. N. Lemon, 'Descending Pathways in Motor Control', Annual Review of Neuroscience, vol. 31, pp. 195–218, Jun. 2008.

[46] K. Amunts et al., 'The coming decade of digital brain research - A vision for neuroscience at the intersection of technology and computing', Zenodo, 2022.